Flow Measurement and Instrumentation

Flow Measurement and Instrumentation 18 (2007) 129–138

Turbulence statistics of flow due to wave–current interaction

B.S. Mazumder*, Satya P. Ojha

Fluvial Mechanics Laboratory, Physics and Applied Mathematics Unit, Indian Statistical Institute, Kolkata-700108, India

Abstract

The paper describes an experimental study carried out in a laboratory flume with a smooth surface to investigate the interactions of gravity waves and unidirectional current. The observations are particularly focused on the changes induced in the mean velocity profiles, turbulent intensity and turbulent shear stress due to superposition of different frequency of waves on turbulent flow. Quadrant analysis has been adopted to investigate the importance of events contributing to the Reynolds shear stress in the near bed region. It is observed that near the boundary the contribution to the total shear stress due to ejection and sweeping events changes with the superposition of waves. The mean time intervals of occurrence of both ejection and sweeping events are obtained from the measurements of fractional contributions to the total shear stress. The distribution of the time interval is found to change as a consequence of superposition of waves. The motivation of this study is to identify the changes of mean flow and turbulent events and to gain better understanding of the physics of flow due to wave–current interaction, which are responsible for sediment transport.

Keywords: Wave-maker; Wave-current interaction; Acoustic Doppler velocimeter (ADV); Stress fraction; Conditional sampling; Log-normal distribution

1. Introduction

The combined presence of waves and currents governs many physical processes of interest to oceanographers and engineers working in coastal zone. In coastal and estuarine regions, waves and current often coexist creating a very effective agent for resuspension and transportation of sediment. The influence of the wave motions on the bed can cause significant quantities of sediment to be suspended above the bed, where it is then transported with the horizontal component of the flow. It has been a subject of great many researchers due to its immense practical significance. Grant and Madsen [1] developed a theoretical model to describe the combined wave–current flow in the vicinity of a rough boundary, predicting an apparent increase in bed roughness and shear stress. They used a time invariant one-layer turbulent eddy viscosity model, which increases linearly with height above the sea bottom. Brevik [2] and Myrhaug [3] extended the one-layer eddy viscosity model proposed by [1] to a two-layer time invariant model and developed analytical solution for the velocity profiles in the rough turbulent boundary layers. The theoretical models for the combined wave–current boundary layer near the rough beds based on time invariant eddy viscosity and mixing length have been described by many researchers [4–9] and others. Although a number of theoretical work has been carried out to study the rough turbulent wave boundary layer flow with zero mean, there have been a relatively little attention on the experimental studies for combined wave–current driven flows concerning the turbulence statistics, despite the fact that such effect has greater importance in practice.

Kemp and Simons [10] provided the experimental data for wave–current interaction over the rough and smooth boundaries; and a considerable increase in bed shear stress and roughness scale was observed at the rough boundary. Subsequently, Kemp and Simons [11] studied the combined wave–current driven flow when the waves propagate against the current over the smooth and rough beds to compare the results with those obtained with waves on the following current. They found that the rate of wave attenuation is increased by the superposition of opposing current and reduced by the following current. Jensen et al. [12] measured velocity and shear stress in laminar, transitionally turbulent and smooth, transitionally rough, and rough turbulent oscillatory boundary

Nomenclature

u, v, w	velocities in Cartesian coordinates
$\bar{u}, \bar{v}, \bar{w}$	time-averaged velocities in Cartesian coordinates
u', w'	fluctuations in u and w
x, y, z	Cartesian coordinates
h	flow depth
u_*	friction velocity
u_m	maximum velocity
g	acceleration due to gravity
Q	flow discharge
Re	Reynolds Number
ν	molecular viscosity of the fluid
κ	von Karman constant
ω	wave frequency
$\langle\rangle$	conditional average
H	hole size
$S_{i,H}$	stress fraction due to ith quadrant corresponding to hole size H
T	Time interval between two turbulent events
$\bar{T}$	mean time interval of turbulent events

layers. Marin [13] performed the experiments for combined wave–current flows over a rippled bed to determine the turbulent velocity distributions when the waves propagate against the current. The significant contribution was that the superposition of waves on the current led to increase the apparent roughness of the bed with increasing wave height and the turbulence intensity over the rippled bed appeared to vary inversely with height at sufficiently large distance from the bed. Recently Mazumder and Ojha [14] carried out an experimental study to investigate the changes in near bed turbulence in combined wave–current flow.

The main objective of the present paper is to describe the experiments performed with the aim of studying the mean velocity and the turbulence statistics due to superposition of waves on the flow. The data collected in the flume studies are particularly analysed to determine the changes induced in the velocity, Reynolds stress and the contributions of turbulent bursting events to the total shear stress above the bed surface. The motivation of this study is to identify the relative importance of mean flow and turbulent events associated with the burst-sweep cycles in the near-bed region due to wave–current interaction, which are responsible for the process of sediment pickup, grain sorting and transportation.

2. Experimental setup

The experiments were carried out in specially designed re-circulating flume [15] at the Fluvial Mechanics Laboratory, Physics and Applied Mathematics Unit, Indian Statistical Institute, Kolkata. Both experimental and re-circulating channels of the flume are of the same dimensions (10 m long, 0.5 m wide and 0.5 m deep). The experimental walls of the flume are made of perspex windows for a length of 8 m, affording a clear view of the flow. One centrifugal pump providing the flow is located outside the main body of the flume. The inlet and outlet pipes are freely suspended from the overhead structure to allow the tilting of the flume. The outlet pipe is fitted with one electromagnetic discharge meter, one by-pass pipe and a valve, so that by adjusting the valve in the outlet, the flow can be controlled at a desired speed. Two honeycomb cages are placed in front of the outlet pipe to ensure the smooth, vortex free, uniform flow of water through the experimental channel. In order to assure the establishment of fully developed flow, measuring section is chosen at a distance of 6 m downstream from the entrance.

A piston-type wave-maker is placed at upstream end of the flume to generate surface waves (Fig. 1). The wave-maker is fabricated in the institute workshop. Two six-inch wheels are fitted at the end of a spindle, which has got a gear in its middle position. One crank and shaft is connected at the rim end of each wheel. The shafts are allowed to pass through a guide to restrict their motion in vertical direction only. A six-inch PVC cylinder (closed at both ends) is fitted at the other ends of the shafts. When the spindle is rotated with the help of motor, the cylinder moves to and fro in the vertical direction. The wave maker is placed in such a way that the cylinder remains partially submerged in the water when it is at its extreme positions — topmost and lowermost. This is done to avoid the generation of small unwanted waves and disturbances. The amplitude of oscillations is maintained at

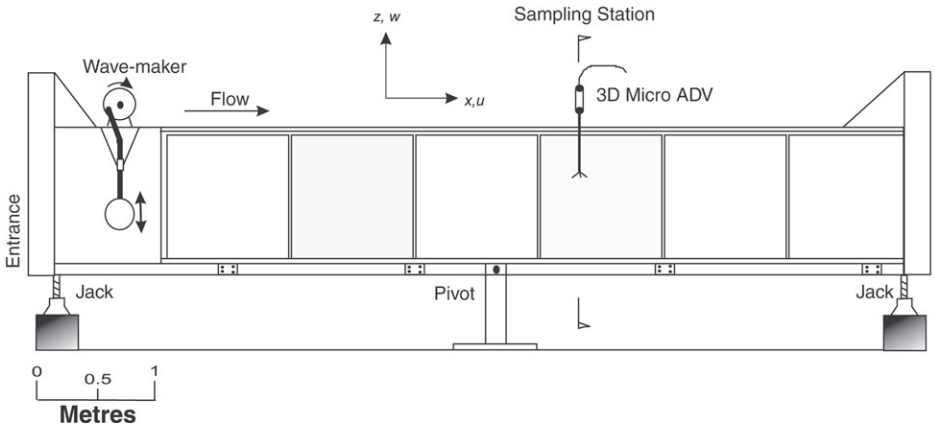

Fig. 1. Schematic diagram of the flume.

11 cm. The oscillations are produced at right angle to the steady unidirectional current. Wave-maker is fixed with a Variac to control the frequency of oscillation. A scale is calibrated using tachometer to make the frequency variation more precise. The coordinate system of the measurement is as follows: x positive downstream and z positive upward. The velocity measurements are obtained by means of 16 MHz *Sontek* 3D-Micro Acoustic Doppler Velocimeter (ADV) at the centerline of the channel with or without surface waves. An only three axis downward-looking probe was used. No measurement near the free surface was made in the present study. ADV is high precision instrument that measures all three components of velocity with fluctuations. The sampling volume is located approximately 5 cm below the transmitter probe; the precise distance depends on individual probe geometry. The sampling volume is an approximately cylindrical volume oriented along the transmitter beam axis. It has a diameter equal to that of the 6 mm ceramic of the transmitter [16,17]. The size of the sampling volume for 16 MHz ADV is 0.09 cm^3. The ADV operates using a Doppler backscattering technique known as pulse-to-pulse coherent Doppler technique [18]. In this technique, the instrument sends two pulses of sound separated by a time lag; it then measures the phase of the return signal from each pulse. The change is the phase divided by the time between pulses is directly proportional to the velocity of the particles in the water. Pulse coherent processing is used because it provides the best possible spatial and temporal resolution. Under good operating conditions, the leading edge of the sampling volume can be placed within about 1 mm of a boundary for 16 MHz ADVs. Factory calibration of the ADV is specified to be 1.0% [17]. The ADV has been validated with several other devices by various authors and has been used in a variety of applications for turbulence measurements, such as over dunes [19] and in the surf zone [20,21].

The velocity data are collected at the rate of 40 Hz for 5 min with the lowest point in each profile being 0.46 cm above the bed surface, highest point being about 24 cm for each profile. Five experiments are performed with different frequency of oscillations of wave maker ($\omega = 0.0, 0.5, 1.0, 1.5, 2.0$ Hz) generating surface waves, superimposing on the unidirectional current. Table 1 provides the experimental details of all five experiments. The mean flow depth is kept constant at 30 cm for all tests. For each experiment, the velocities are measured at the centerline at about 24 vertical positions. Here, the experiments are performed at a discharge $Q = 0.04$ cubic m/s, the Reynolds number $Re = u_m h/\nu = 1.50 \times 10^5$; and the Froude number $u_m/\sqrt{gh} = 0.29$, where the friction velocity $u_* = 2.1$ cm/s and u_m (=50 cm/s) is the maximum velocity observed at the height $z = 24$ cm above the bed surface. The experiment with zero frequency of waves corresponds to the current alone.

3. Experimental results and discussions

3.1. Results from current alone experiments

For the instantaneous velocity components (u, v, w) in the (x, y, z)-directions, the following three relations can be written as

$$u = \bar{u} + u', \quad v = \bar{v} + v' \quad \text{and} \quad w = \bar{w} + w', \tag{1}$$

where over bar denotes time-averaged velocity and the prime denotes its fluctuations. The vertical profiles of mean velocity components $(\bar{u}, \bar{v}, \bar{w})$ illustrate the characteristic features of the flow over the plane surface. To ensure the fully developed flow at the sampling station we performed three experiments at three different locations in the downstream direction and found no change amongst the results of those tests. In all three tests with unidirectional current the mean vertical velocity is found to be almost zero throughout the depth of the flow. Fig. 2(a)–(d) shows the streamwise mean velocity, streamwise turbulent intensity, vertical turbulent intensity and Reynolds shear stress profiles for current alone. The data is normalized by the friction velocity which is calculated from the log law. The logarithmic mean velocity profile was found to follow the universal law of wall (inset Fig. 2(a)). The intensity of turbulence ($\frac{\sqrt{\overline{u'^2}}}{u_*}$) in the stream-wise direction or the root mean squared (rms) values of turbulent fluctuating velocity (u') is also computed from the velocity measurements. The high turbulence intensity is often used as an indicator of the flow potential for erosion and suspension of sediment particles. The Reynolds shear stress component ($-\overline{u'w'}/u_*^2$) is computed and it exhibits the same features as seen in the turbulent intensity profiles. It is observed that the Reynolds shear stress increases and reaches a maximum value at a distance near the bed and then decreases towards the free surface. The results are in good agreement with the previous investigations [10,22].

Table 1
Experimental data

Exp. no.	Wave frequency (Hz)	Wave height (cm)	Depth of flow (cm)	u_* (cm/s)
1	0	–	30	2.10
2	0.5	1	30	2.45
3	1.0	3	30	2.66
4	1.5	7	30	2.22
5	2.0	10	30	2.03

3.2. Mean velocity and turbulence for combined wave and current

In order to estimate the mean flow under the wave–current interactions, four different experiments were performed superimposing the waves of different frequency of oscillations on the unidirectional current. Time series of the 10 s velocity record of the experiments are presented in Fig. 3 for three different values of frequency. The superposition of waves changes significantly the mean flow and turbulence characteristics and at the same time the increase of the wavelength and decrease of wave height are observed due to unidirectional flow when these are compared with that generated from the waves alone. The increase of frequency of oscillation at the wave maker leads to decrease the wavelength and to increase the wave height at the free surface. Fig. 4(a)–(d) are presented to show a comparative study of stream-wise mean

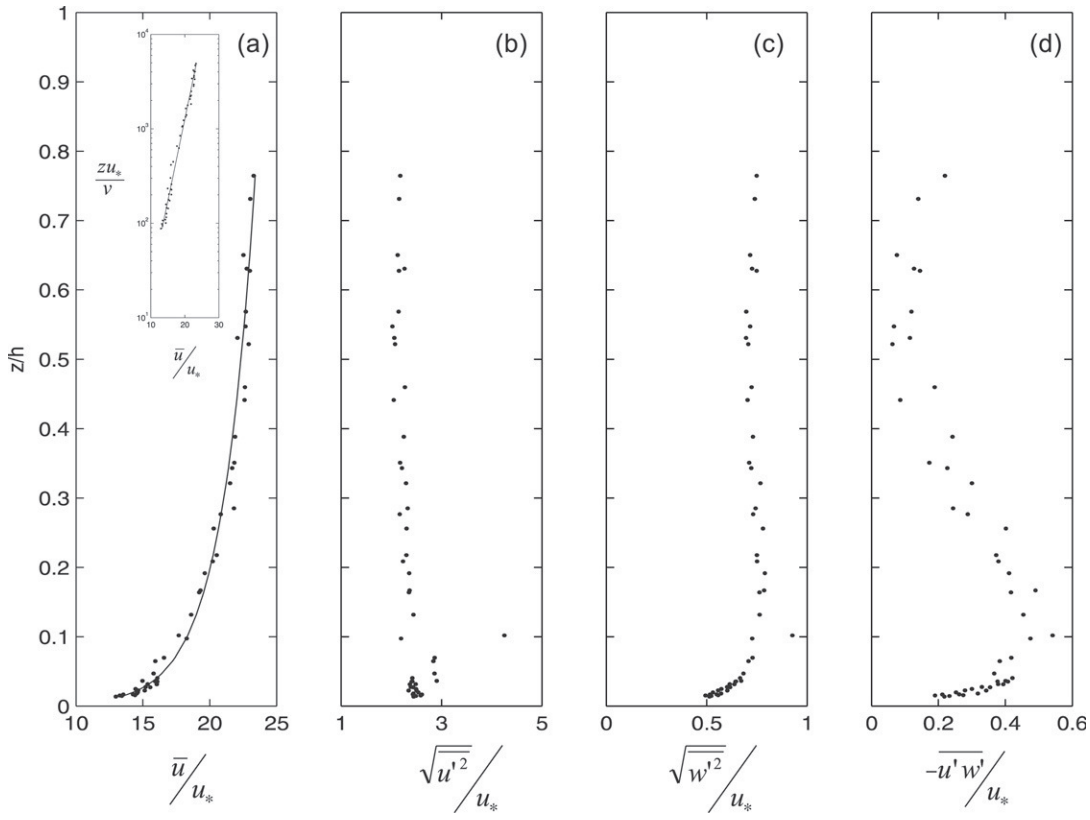

Fig. 2. (a) Normalized streamwise mean velocity, (b) normalized streamwise turbulent intensity, (c) normalized vertical turbulent intensity and (d) normalized Reynolds shear stress plots for current alone test.

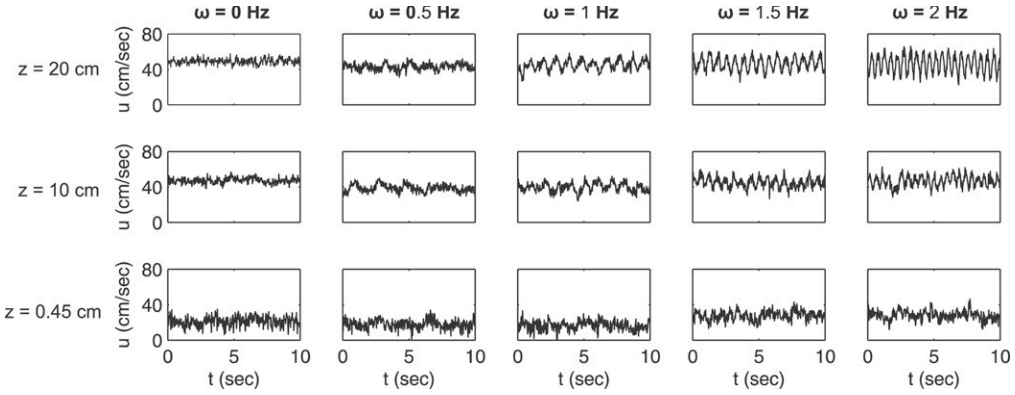

Fig. 3. 10 s stream-wise velocity record for the five experiments at three different heights.

velocity profiles for combined wave–current flow with that of current alone. Results show that when the waves of 0.5 Hz frequency are introduced to the flow a remarkable reduction in the mean flow is observed for the whole depth but the structure of the profile remains logarithmic (Fig. 4(a)). It is also seen from the figure that profiles get shifted parallel towards left to the profile of current alone. Further reduction in mean velocity is observed with the addition of the waves of frequency 1 Hz (Fig. 4(b)). The 1.5 Hz frequency of wave produces no further decrease in mean velocity, however the profile has the tendency to fall back to the profile of the current alone experiment (Fig. 4(c)). Although the mean velocity is less throughout the depth as compared to the current alone, but it is more than that of 0.5 and 1 Hz frequency of waves. Further increase in frequency of 2 Hz shows a remarkable increase in mean velocity in the region $z/h < 0.4$ and decrease in velocity in the region $z/h > 0.4$ (Fig. 4(d)). There is a certain frequency of oscillation for which the wave-induced mean velocity collapses with that of current alone. The friction velocity is calculated by fitting the log law to the velocity profile. Results show that the friction velocity increases with frequency of waves and reaches the least value with 2 Hz frequency of waves. There is a critical frequency for which the friction velocity generated due to wave–current interaction is minimum.

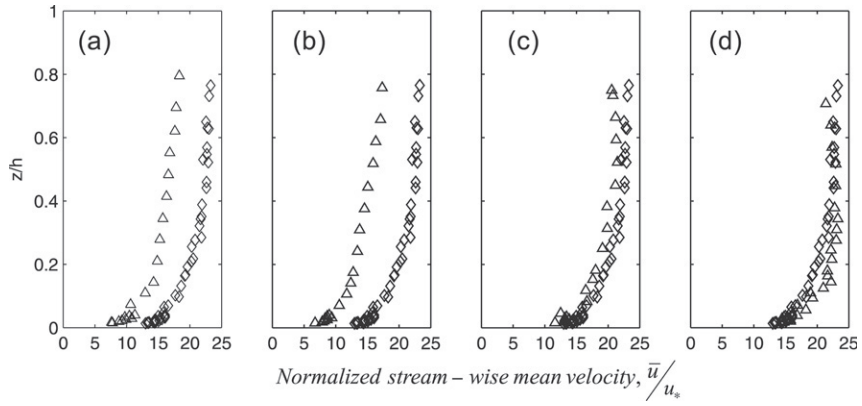

Fig. 4. (a)–(d) Normalized streamwise mean velocity profiles for combined wave–current experiments. (a) to (d) represent velocity profiles for $\omega = 0.5$ Hz, $\omega = 1.0$ Hz and $\omega = 2$ Hz respectively. Velocity profile for current alone is also plotted for reference (symbol $\diamond$).

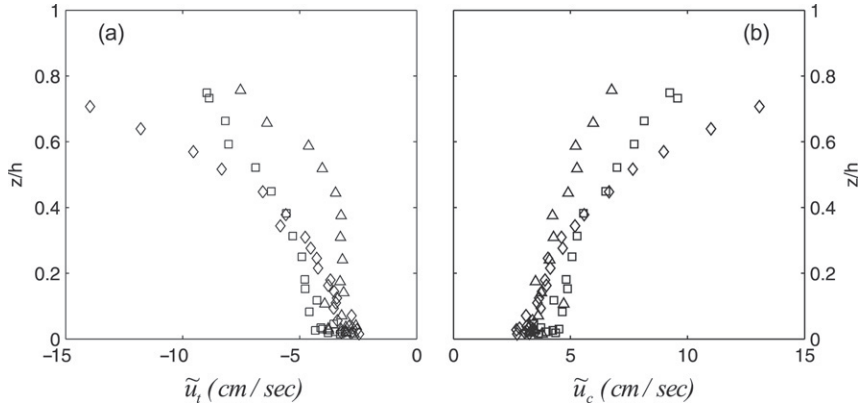

Fig. 5. (a), (b) Stream-wise velocity profiles corresponding to the passage of wave crest and trough for three combined wave–current tests. Symbols, $\triangle$: $\omega = 1$ Hz; $\square$: $\omega = 1.5$ Hz; $\diamond$: $\omega = 2$ Hz.

Analysis of combined wave–current interacting flow is carried out by computing the average of the wave-induced velocity at phases corresponding to the passage of wave crest and trough. We define the average velocity $\tilde{u}_c$ as

$$\tilde{u}_c = N^{-1} \sum_{i=0}^{N} u_{c_i} - \bar{u} \tag{2}$$

where $\tilde{u}_c$ is the average velocity at the phase corresponding to the passage of wave crest, u_{c_i} is the value of u at ith crest, $\bar{u}$ is the mean value over the full sample period and N is the number of observations during the total time. Similarly we define average velocity $\tilde{u}_t$ at the phase corresponding to the passage of trough. The streamwise mean velocity profiles at phases corresponding to the passage of wave crest and trough for the different frequency of oscillation ($\omega = 1, 1.5, 2$ Hz) are shown in Fig. 5(a), (b) and for vertical mean velocity profiles in Fig. 6(a), (b). The data of the frequency 0.5 Hz do not have any single dominating frequency appearing in the velocity record. The magnitudes of the stream-wise and vertical mean velocities are more at the phase corresponding to the wave trough as compared to that at the phase corresponding to the wave crest. This phenomenon is consistent for all the frequency of waves.

The normalized Reynolds shear stress ($\frac{-\overline{u'w'}}{u_*^2}$) for all combined wave–current tests are plotted in Fig. 7(a)–(d); and are compared with that of unidirectional current alone. It is seen from the Fig. 7(a), (b) that the superposition of waves of frequency 0.5 and 1 Hz causes a considerable reduction in the turbulent shear stress near the boundary and increase in the outer flow. With the waves of frequency 1.5 Hz (Fig. 7(c)) the shear stress increases almost linearly in the near bed region and then decreases in the outer flow. For the wave frequency of 2 Hz, the shear stress profile again acquires the same shape as in current alone and reaches a maximum value 0.7, which is greater than the current alone (Fig. 7(d)). The peak in the turbulent shear stress profile shifts towards the main flow for the waves of frequency 0.5 Hz and reaches a maximum at 1 Hz; and then it moves towards bottom boundary with further increase of wave frequency. In the 2 Hz frequency, the peak is observed almost at the same height as in current alone. The change of shear stress with frequency of wave may be attributed to the vortices generating due to wave superposition. The upper half of the vortex has motion in the flow direction while the lower half moves in the direction opposite to the flow, so the upper half of the vortex helps to increase the shear stress while the lower half has the tendency to decrease. The diameter of the vortices is almost equal to the flow depth for 1 Hz frequency test

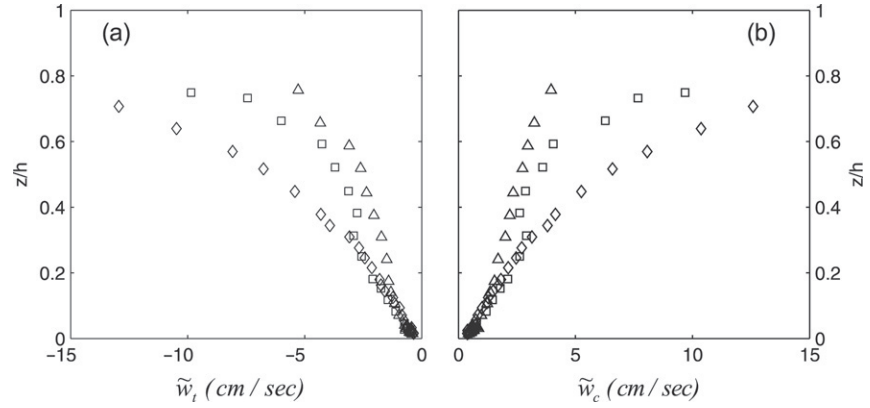

Fig. 6. (a), (b) Vertical velocity profiles corresponding to the passage of wave crest and trough for three combined wave–current tests. Symbols, △: $\omega = 1$ Hz; □: $\omega = 1.5$ Hz; ◇: $\omega = 2$ Hz.

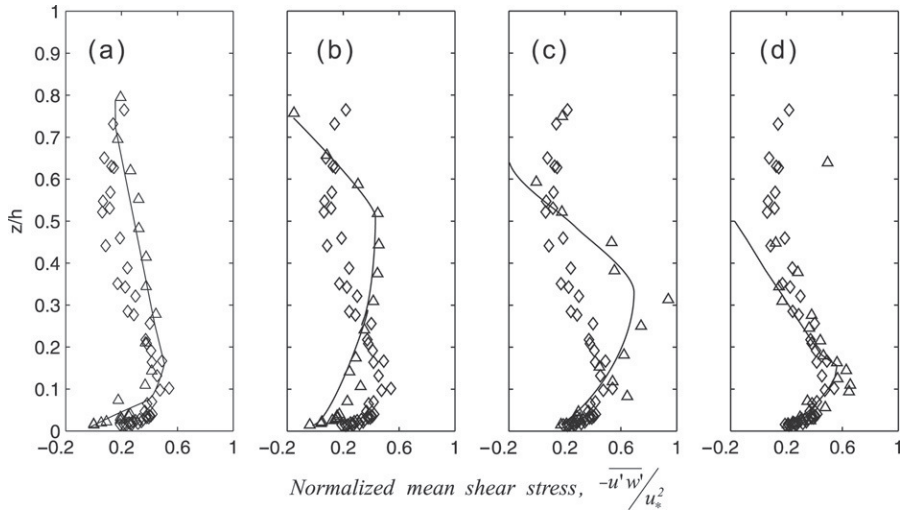

Fig. 7. (a)–(d) Mean Reynolds shear stress profiles for combined wave–current experiments. (a) to (d) represents profiles for $\omega = 0.5$ Hz, $\omega = 1.0$ Hz, $\omega = 1.5$ Hz and $\omega = 2$ Hz respectively. Shear stress profile for current alone is also plotted for reference (symbol ◇).

and hence shear stress is changed almost throughout the depth and the maximum shear stress is obtained at about $z/h = 0.5$. As the frequency increases the vortex diameter decreases and thus the vertical extent to which the shear stress is affected also decreases.

Due to the insignificant periodicity observed in near-bed region, the whole depth of flow is designated into two regimes, namely the wave dominated (outer regime) and the current dominated regime (near-bed region). Wave dominant regime lies in the upper region ($z/h > 0.3$), whereas the current dominant region lies near boundary ($z/h < 0.3$) (Figs. 5 and 6). The figures reveal that the increasing frequency of waves leads to increase of wave dominated region. Although there is no precise boundary identifying two distinct regimes we have designated them based on the periodicity of frequency content of the velocity signals. Figs. 5 and 6 shows that the ensemble average velocity does not change with varying wave frequency near boundary ($z/h < 0.3$). As the flow near the bottom is current dominated, the quadrant wise analysis of the flow is performed at three different heights, which is presented in the following section.

3.3. Conditional statistics of the Reynolds stress

Wall turbulence is controlled by the presence of vortices organized in space and time, called coherent structures, which are responsible for most of the resistance to motion and the transport process. These structures are quasi-periodic and occupy the whole boundary layer depth. The smooth wall region including the viscous sublayer and adjacent buffer layer has been shown to be characterized by a randomly occurring 'burst-sweep cycle' in which low speed fluid near wall is ejected violently. Reynolds stress contributions and turbulence productions are associated with these turbulent events as shown with conditional sampling techniques [23,24]. The turbulent events are defined by the four quadrants as outward interactions ($i = 1; u' > 0, w' > 0$), ejections ($i = 2; u' < 0, w' > 0$), inward interactions ($i = 3; u' < 0, w' < 0$), and sweeps ($i = 4; u' > 0, w' < 0$). At any point in a stationary flow, the contribution to the total Reynolds stress from quadrant i, excluding a hyperbolic hole region of size H, is

$$\langle u'w' \rangle_{i,H} = \lim_{T \to \infty} \frac{1}{T} \int_0^T u'(t)w'(t) I_{i,H}(u', w') \mathrm{d}t \tag{3}$$

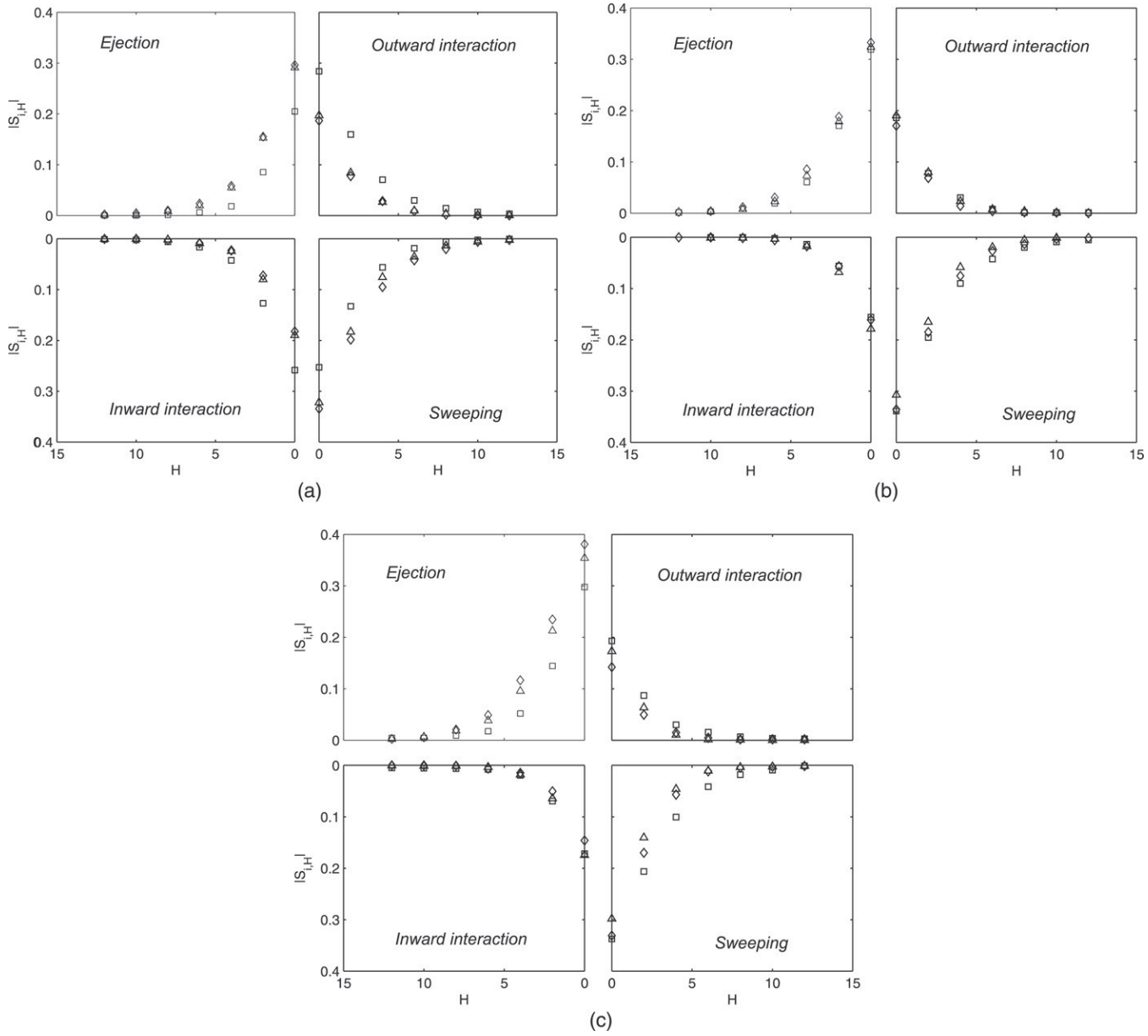

Fig. 8. (a)–(c) Stress fraction plotted against hole size H. (a) For $z/h = 0.015$, (b) for $z/h = 0.07$ and (c) for $z/h = 0.17$. Symbols, △: $\omega = 1$ Hz; □: $\omega = 1.5$ Hz; ◇:$\omega = 2$ Hz.

where the angle brackets denote a conditional average, and the indicator function $I_{i,H}$ obeys

$$I(u', w') = \begin{cases} 1, & \text{if } (u', w') \text{ is in the } i\text{th quadrant and if} \\ & |u'w'| \geq H\overline{|u'w'|} \\ 0, & \text{otherwise.} \end{cases} \quad (4)$$

Here H is the threshold parameter in the Reynolds stress signals, which enables us to extract those values of $u'w'$ from the whole set of data, which are greater than H times $\overline{|u'w'|}$ value. The value of H gives us an idea of the strength of the event. The expression $|u'w'| \geq H\overline{|u'w'|}$ can be thought of as a filter which filters out those signals whose strength is less than H times $\overline{|u'w'|}$. The threshold parameter H is used here to get an idea of the relative importance of various quadrant events in generating shear stress of a particular strength. The stress fraction by ith quadrant defined above is

$$S_{i,H} = \langle u'w' \rangle_{i,H} / \overline{|u'w'|} \quad (5)$$

$$\sum_{i=1}^{4} |S_{i,0}| = 1. \quad (6)$$

Although the periodic disturbance due to wave maker is unable to induce sinusoidality in the velocity signals near the bottom but it certainly changes the flow dynamics there, which is revealed by the stress fraction plots in Fig. 8(a)–(c). Figures show the stress fraction $S_{i,H}$ plotted against the hole size H for each of the four quadrants in the (u', w') plane for three dimensionless heights $z/h = 0.015$, 0.07 and 0.17. These plots clearly show the effect of superposition of waves on the current.

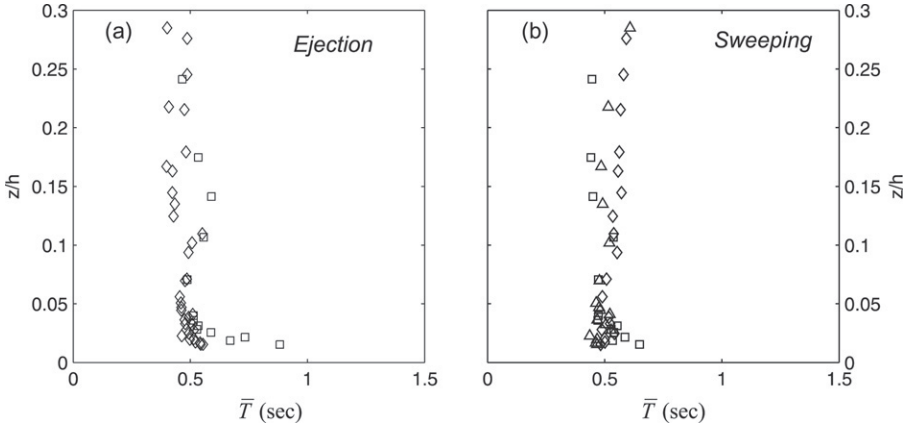

Fig. 9. Mean time interval of occurrence of bursting events for $H = 2$, (a) ejection, (b) sweeping. Symbols, △: $\omega = 1$ Hz; □: $\omega = 1.5$ Hz; ⋄: $\omega = 2$ Hz.

In the current alone experiment ($\omega = 0$) the bursting events are dominant over the two interaction events each contributing almost equally for $H = 0$ ($S_{2,0} \approx 0.30$, $S_{4,0} \approx 0.33$) near the boundary, $z/h = 0.015$ (Fig. 8(a)). The contribution due to outward and inward interactions at this height is about 18 percent ($S_{1,0} \approx S_{3,0} \approx 0.185$). With the wave of 1 Hz frequency, the contributions due to ejection and sweeping events decrease, while that due to interaction events increase. The outward interaction contributes about 30% ($S_{1,0} \approx 0.30$) while inward interaction contributes 26% ($S_{3,0} \approx 0.26$). For $H = 0$, contribution from the second and fourth quadrant reduces to 19% and 25% respectively. Further increase in frequency ($\omega = 2$ Hz) leads to reduce the contribution to the total shear stress due to interaction events and to increase the contribution due to bursting events. Figures reveal that the contributions to the total shear stress due to the four quadrant events for the frequency of 2 Hz are almost the same as in the current alone.

The transport process is almost symmetric in the pair of opposite quadrants for the current alone ($\omega = 0$) at $z/h = 0.07$ and the symmetry is retained even after the superposition of waves (Fig. 8(b)). Although the superposition of waves changes the transport process as compared with the current alone, but no substantial change is observed with varying frequency of waves. For the current alone, both the interaction events contribute equally about 16% ($S_{1,0} \approx S_{3,0} \approx 0.16$) while ejection and sweeps both make a contribution of 34% for $H = 0$.

At height $z/h = 0.17$ the transport process with varying wave frequency is same as observed at $z/h = 0.015$ (Fig. 8(c)). The inward and outward interactions contribute symmetrically ($S_{1,0} \approx S_{3,0} \approx 0.15$) while ejection contribute about 37% and sweeping about 33% to the total shear stress in the current alone test. Both interaction events cease to contribute for $H > 5$. The superposition of waves of 1 Hz frequency leads to reduce the stress fractions of ejection events, while it increases the stress fractions of both the interaction events. The contribution due to sweeping gets increased and the relative increase is observed to be more with increasing hole size H. Further increase in wave frequency reduces the stress fraction due to outward interaction and sweeping events. The contribution to the shear stress due to ejection gets increased but it remains less as compared with the corresponding contribution in current alone tests, while no change in the stress fraction is observed due to inward interaction.

3.4. Time scales of ejection and sweeping events

The ejection and sweeping events can be sorted out from the whole data for a particular threshold value H by filtering the data according to the condition $|u'w'| \geq H\overline{|u'w'|}$. Since the data set contains time record, one can obtain the corresponding time of events. For $H = 2$ the mean time interval $\bar{T}$ of occurrence of ejection and sweeping events is calculated and is shown in Fig. 9(a), (b). It is observed from the figures that near the boundary ($z/h \leq 0.04$) the $\bar{T}$ for ejection and sweeping events increases with superposition of wave of 1 Hz frequency, but the increase is more for ejection events compared to sweeping. No change in $\bar{T}$ is observed with waves of 2 Hz frequency when compared with current alone. This implies that the superposition of 1 Hz wave decreases the frequency of ejection and sweeping near the boundary but have no effect in the region away from the boundary. If we compare the relative changes in the time intervals of occurrence of ejection/sweeping events of different frequency of waves with that of current alone, the changes seem to be more in case of ejection events, which means the superposition of waves leads to suppress the frequency of occurrence of ejection.

The probability distributions of the time interval T between two successive ejection (or sweeping) events are computed for three experiments ($\omega = 0, 1, 2$; Hz) at three different heights ($z/h = 0.015, 0.07, 0.17$) and are presented on probability paper in Figs. 10 and 11. The plot gives a straight line for all the experiments at height $z/h = 0.015$ indicating the log-normal distribution of dimensionless time interval for ejection and sweeping both. The qualitative results agree well with those of Rao et al. [25]. The distribution of the time interval deviates from log normality at heights $z/h = 0.07$ and 0.17 for the combined wave current experiments and the deviation is large for large frequency waves.

4. Conclusion

Five experiments, one current alone and four combined wave–current, are carried out to study the changes in the flow structure due to the superposition of waves on the

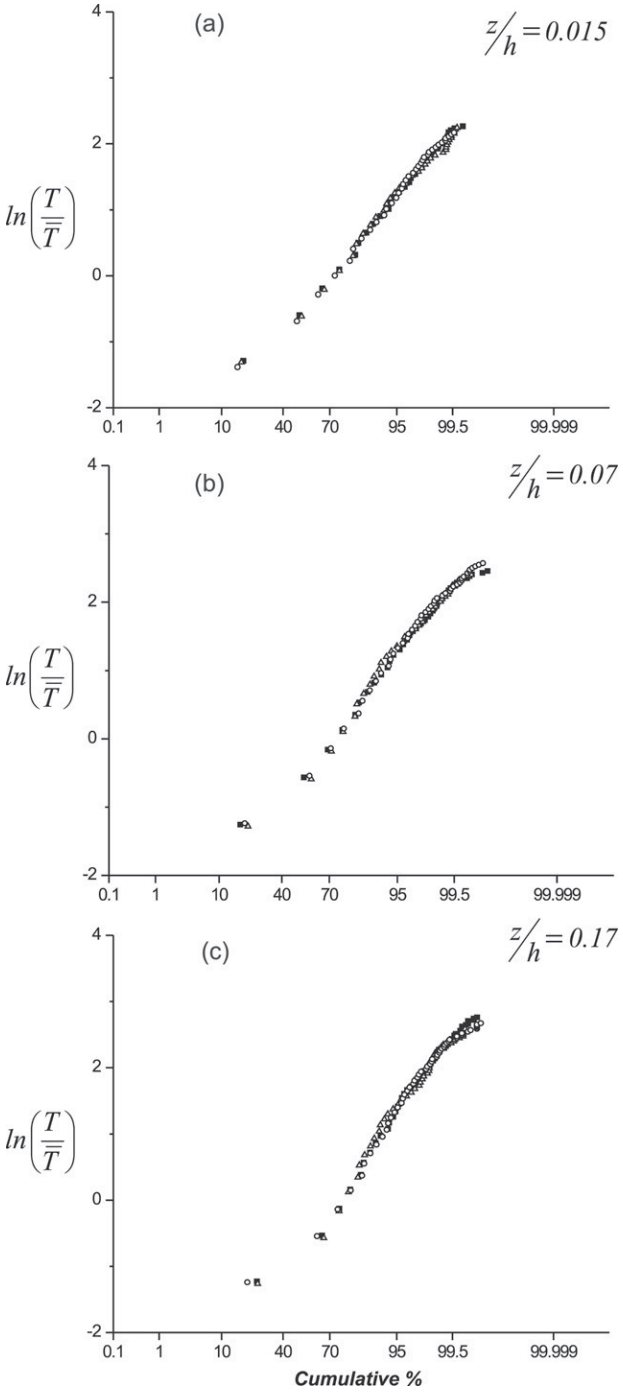

Fig. 10. Distribution of the time interval of occurrence of ejection events plotted on probability graph for different heights and frequency. Symbols, ■: $\omega = 0$ Hz; ○: $\omega = 1.5$ Hz; △: $\omega = 2$ Hz.

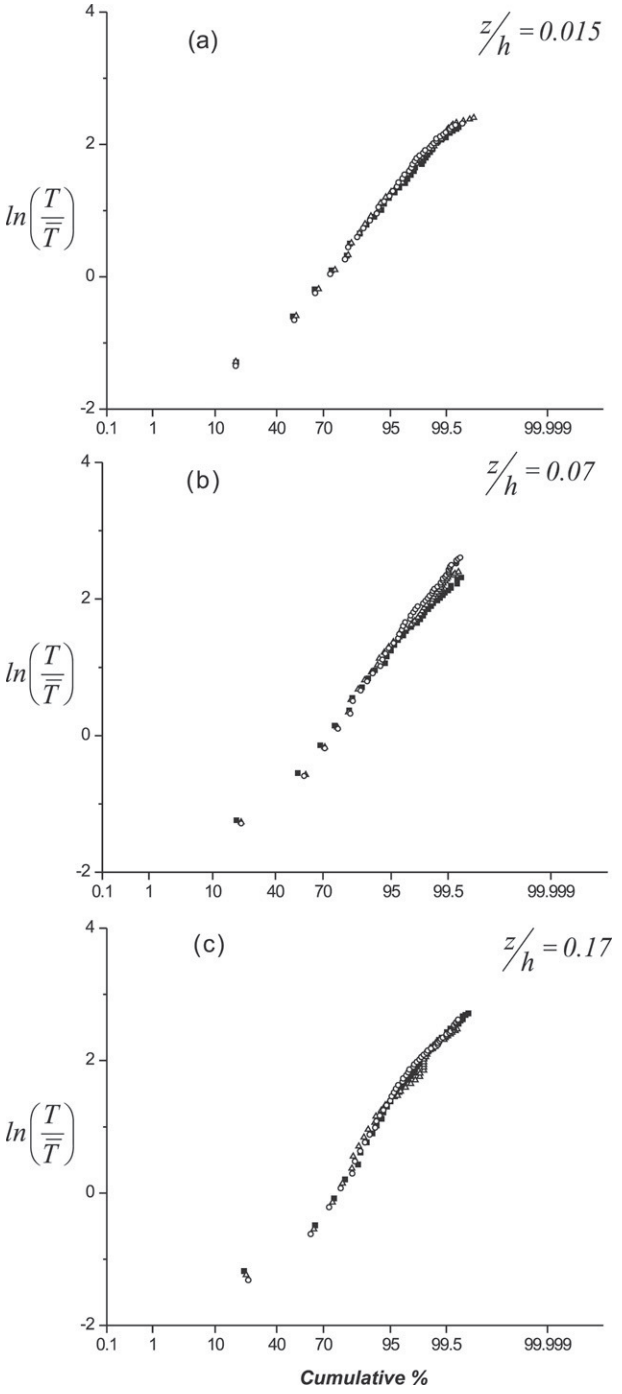

Fig. 11. Distribution of the time interval of occurrence of sweeping events plotted on probability graph for different heights and frequency. Symbols, ■: $\omega = 0$ Hz; ○: $\omega = 1.5$ Hz; △: $\omega = 2$ Hz.

current. The finding reveals that the streamwise mean velocity decreases throughout the depth on the superposition of waves of frequency 0.5 and 1 Hz. Further increase in wave frequency results in increase in the mean velocity and collapses at certain frequency with mean flow of current alone. On addition of waves the mean shear stress near the bed first decreases then increases with varying wave frequency. Quadrant-wise decomposition of the turbulent shear stress shows that near the boundary the contribution to the total shear stress due to ejection and sweeping events decreases with increase in wave frequency. The mean time interval of occurrence of ejection/sweeping events increases with increase in wave frequency, which implies less frequent occurrence of bursting events with wave. Moreover, the time interval of occurrence of ejection and sweeping events follow log normality for all five experiments near the bed but the distribution deviates from log normality at the height $z/h \geq 0.07$ and the deviation increases with increase in wave frequency.

Acknowledgements

The authors would like to thank Professor Mutlu Sumer of DTU for suggesting the design of the wave maker during BSM's visit to their laboratory. They also acknowledge several discussions with Professors J.K. Ghosh and C. Chakraborty and gratefully acknowledge the financial support (No. ESS/23/VES/109/2000) from Department of Science and Technology (DST), New Delhi. Authors wish to acknowledge the anonymous reviewers for their valuable suggestions for bringing the paper into its present form.

References

[1] Grant WD, Madsen OS. Combined wave and current with a rough bottom. Journal of Geophysical Research 1979;84(C4):1797–808.
[2] Brevik I. Oscillatory rough turbulent boundary layers. Journal of Waterway, Port, Coastal and Ocean Engineering, ASCE 1981;107(WW3): 175–88.
[3] Myrhaug D. On a theoretical model of rough turbulent wave boundary layers. Ocean Engineering 1982;9(6):547–65.
[4] Fredsoe J. Turbulent boundary layer in wave–current motion. Journal of Hydraulic Engineering 1984;110:1103–19.
[5] Van Kersteren WGM, Bakker WT. Near bottom velocities in waves with a current: Analytical and numerical computations. In: Proc. 19th int. conf. coastal engineering. ASCE; 1984. p. 1161–77.
[6] Christofferson JB, Jonsson IG. Bed friction and dissipation in a combined current and wave motion. Ocean Engineering 1985;12(5):387–423.
[7] O'Connor BA, Yoo D. Mean bed friction of combined wave/current flow. Coastal Engineering 1988;12:1–21.
[8] Sleath JFA. Velocities and shear stresses in wave–current flows. Journal of Geophysical Research 1991;96(C8):15237–44.
[9] Wiberg PL. A theoretical investigation of boundary layer flow and bottom shear stress for smooth, transitional, and rough flow under waves. Journal of Geophysical Research 1995;100(C11):22667–79.
[10] Kemp PH, Simons RR. The interaction between waves and a turbulent current: Waves propagating with the current. Journal of Fluid Mechanics 1982;116:227–50.
[11] Kemp PH, Simons RR. The interaction between waves and a turbulent current: Waves propagating against the current. Journal of Fluid Mechanics 1983;130:73–89.
[12] Jensen BL, Sumer BM, Fredsoe J. Turbulent oscillatory boundary layers at high Reynolds Numbers. Journal of Fluid Mechanics 1989;206: 265–297.
[13] Marin F. Velocity and turbulence distributions in combined wave–current flows over a rippled bed. Journal of Hydraulic Research 1999;37(4): 501–16.
[14] Mazumder BS, Ojha SP. Near bed turbulence statistics in combined wave–current flow. In: Proc. of national conference on hydraulics. 2005, p. 861–71.
[15] Mazumder BS, Ray RN, Dalal DC. Size distribution of suspended particles in open channel flow over sediment beds. Environmetrics 2005; 16:149–65.
[16] Lohrmann A, Cabrera R, Kraus NC. Acoustic-Doppler velocimeter (ADV) for laboratory use. In: Proc. conf. on fundamentals and advancements in hydraulic measurements and experimentation. 1994, p. 351–65.
[17] SonTek/YSI Technical Notes, SonTek/ YSI, Inc., San Diego. September 1, 2001.
[18] Lhermitte R, Serafin R. Pulse-to-pulse coherent Doppler sonar signal processing techniques. Journal of Atmospheric and Oceanic Technology 1984;1(4):293–308.
[19] Venditti JG, Bennett SJ. Spectral analysis of turbulent flow and suspended sediment transport over fixed dunes. Journal of Geophysical Research 2000;105(C9):2035–47.
[20] Elgar S, Raubenheimer B, Guza RT. Current meter performance in the surf zone. Journal of Atmospheric and Oceanic Technology 2001;18(10): 1735–46.
[21] Trowbridge J, Elgar S. Turbulence measurements in the surf zone. Journal of Physical Oceanography 2001;31(8):2403–17.
[22] Nezu I, Rodi W. Open-channel flow measurements with a Laser Doppler anemometer. Journal of Hydraulic Engineering 1984;112(5):335–55.
[23] Wallace JM, Eckelmann H, Brodkey RS. The wall region in turbulent shear flow. Journal of Fluid Mechanics 1972;54:39–48.
[24] Lu SS, Willmarth WW. Measurements of the structure of the Reynolds stress in a turbulent boundary layer. Journal of Fluid Mechanics 1973;60: 481–511.
[25] Rao KN, Narasimha R, Badri Narayan MA. The 'bursting' phenomenon in a turbulent boundary layer. Journal of Fluid Mechanics 1971;48: 339–52.